Journal of Molecular Liquids 187 (2013) 157–164

Contents lists available at ScienceDirect

Journal of Molecular Liquids

journal homepage: www.elsevier.com/locate/molliq

Dielectric saturation in water as quantitative measure of formation of well-defined hydration shells of ions at various temperatures and pressures. Vapor–liquid equilibrium case

I. Danielewicz-Ferchmin [a], E.M. Banachowicz [a], A.R. Ferchmin [b,*]

[a] Faculty of Physics, A. Mickiewicz University, Umultowska 85, PL-61-614 Poznań, Poland
[b] Institute of Molecular Physics, Polish Academy of Sciences, M. Smoluchowskiego 17, PL-60-179 Poznań, Poland

ARTICLE INFO

Article history:
Received 25 May 2013
Accepted 13 June 2013
Available online 9 July 2013

Keywords:
Water
High electric field
Static electric permittivity
Dielectric saturation
Electrochemistry

ABSTRACT

Static electric permittivity ϵ of water at equilibrium saturated vapor pressures in electric field in the range $10^8 < E < 10^{11}$ V m^{-1} was calculated. A quantitative measure of the dielectric saturation phenomenon was introduced. It is found that, according to the definition of this measure, well-defined first hydration shells of numerous ions investigated by X-ray and neutron scattering methods described in literature are electrically saturated, and that at various conditions. Calculations show that around some ions, including Ag^+, whose hydration shells are not saturated at ambient conditions, dielectric saturation of water can be achieved by increasing temperature and pressure up to the values not far from the critical ones. This is compared with extended X-ray absorption fine structure (EXAFS) and XAFS data for Ag^+ and Rb^+ found in literature.

1. Introduction

Studies of ion hydration at elevated temperature T and pressure P are of importance to geochemistry [1,2]. They are also valuable in electrochemistry, e. g., when one looks for partial molar volumes of ions in aqueous solutions [3]. On the other hand, our limited knowledge of the behavior of water in very high electric field E of the order of ~1 GV m^{-1} calls for such studies. At the same time, experimental works on that topic are scarce due to technical difficulties and it seems worthy to look more closely at the properties of ionic hydration shells in such conditions.

It should be noted that the knowledge of static electric permittivity ϵ is needed for finding many physical parameters of water in high field E, for example entropy, the related electrocaloric effect, as well as local electrostriction and electrostriction pressure in hydration shells, to mention but a few. Some of the values of ϵ in high E are available in literature: those at ambient conditions [4], under ambient pressure at varied temperature [4] and at ambient T but under varied P [5]. Also, ϵ of water at equilibrium with vapor (at various T and P) was calculated [6].

Two main topics will be pursued. Firstly, the question is raised: what are the dielectric properties of water in the field of the ions at elevated temperature and pressure? In particular, what are the conditions of its dielectric saturation characterized as the state in which the H_2O dipole moments point toward (or out of) the ion center? To answer these questions, some ϵ data taken from the preliminary short account [6] will be recalled for consistency and used herein as a basis for further development devoted to finding conditions for dielectric saturation. A quantitative measure of the dielectric saturation will be introduced as a special value of $\langle\cos\theta\rangle$ — the mean cosine of the angle θ between the direction of the dipole moment $\boldsymbol{\mu}$ of a H_2O molecule and the direction of the electric field $\boldsymbol{E}$. The dielectric saturation state of water corresponds to the values of $\langle\cos\theta\rangle$ very close to unity, to be precisely defined later. The discussion is based on the statistical approach [4,5] taking into account the dipoles of water molecules as well as the presence of hydrogen bonds. This approach is applicable to static electric permittivity ϵ of water in high electric field and in temperature and pressure ranges in which H_2O is liquid.

Secondly, the dielectric saturation phenomenon in the hydration shells of ions will be confronted with the knowledge, available in literature, on the character of the shells obtained by methods using X-rays and neutrons. It will be noted that well-defined hydration shells around many ions are characterized, at the same time, by the dielectric saturation state of water.

It will be argued that ions can be categorized on the one hand as cations with two or three excess elementary charges, e.g., Ni^{2+} or Cr^{3+}, which form well-defined hydration shells characterized by two resolved peaks in the radial distribution function [7,8], with addition of Li^+ ions and on the other hand by other cations and anions with one excess elementary charge revealing no such shells. At ambient conditions,

* Corresponding author. Tel.: +48 61 8695213; fax: +48 61 8684524.
E-mail address: arfer@ifmpan.poznan.pl (A.R. Ferchmin).

0167-7322/$ – see front matter © 2013 Published by Elsevier B.V.
http://dx.doi.org/10.1016/j.molliq.2013.06.005

the dielectric properties of hydration shells around either category of ions mentioned above were already analyzed [9]. Herein, they will be characterized as either electrically saturated or not, respectively. Note that the electrically saturated shells are at the same time highly compressed by the ionic electric field [3] or, more precisely, due to the huge electrostriction under local electrostriction pressure [9]. It is likely that such local objects as hydration shells can serve as distinct scatterers to X-rays or neutrons, in particular if they are more dense than the rest of the solvent. This is the case if $\langle\cos\theta\rangle$ is very close to unity, that is in the state of dielectric saturation [9].

It will be shown that even around ions with no well-defined hydration shells and no dielectric saturation in their first hydration shells at ambient conditions, as exemplified by Ag^+ and Rb^+, dielectric saturation can be reached at elevated temperature and pressure not far from the critical conditions. This indicates the possibility of well-defined hydration shell formation in the latter case. The T and P values at vapor–liquid water equilibrium were chosen in our calculations because the measurements on Ag^+ aqueous solutions were taken at equilibrium saturated vapor pressures [10].

It is known that the freezing point [11] and the critical point [1] as well as the phase equilibrium of water in general [12,13] are shifted in high electric field. In particular, it concerns the vapor–liquid water phase boundary. For this reason, the vapor–liquid water phase boundary not in the field and that in the field should be distinguished. Herein, we choose the T and P variables taken along the vapor–liquid water phase boundary existing outside the field.

2. Static electric permittivity $\epsilon(P, T, E)$ – theory

Let us start with the calculation of the static electric permittivity $\epsilon(P, T, E)$ data for T and P values taken from the vapor–liquid phase boundary (cf. Ref. [14]) with the electric field strength E as a parameter. To relate the electric permittivity ϵ with the dipole moment $\boldsymbol{\mu}$ of a molecule, a statistical mechanical calculation is applied leading to $\langle\cos\theta\rangle$ — the mean cosine of the angle θ between the direction of the dipole moment $\boldsymbol{\mu}$ of H_2O molecule and the direction of the electric field $\boldsymbol{E}$. In water, due to the presence of the hydrogen bonds, the number I of admitted orientations of the dipole moment $\boldsymbol{\mu}$ of a molecule of water with respect to the direction of the electric field is limited. The value of $\langle\cos\theta\rangle$ for an arbitrary number I of orientations of a dipole is expressed by the function [4]

$$\langle\cos\theta\rangle = B_I(\Xi) \tag{1}$$

where

$$B_I(\Xi) = \frac{I}{I-1}\coth\frac{I\Xi}{I-1} - \frac{1}{I-1}\coth\frac{\Xi}{I-1}, \tag{2}$$

where Ξ is defined in Eq. (3)

$$\Xi = \frac{\mu E_{On}}{kT}, \tag{3}$$

where E_{On} is the component of the Onsager local field (cf. Ref. [15], Chapter V) parallel to the vector $\boldsymbol{E}$ acting on the dipole moment $\boldsymbol{\mu}$ and k denotes the Boltzmann constant. The value of the external electric field E is related with the $\boldsymbol{E}_{On}$ as follows:

$$E_{On} = \frac{\epsilon\left(n^2+2\right)}{2\epsilon+n^2}E, \tag{4}$$

where n denotes the refraction index. For integer I, $B_I(\Xi)$ as defined in Eq. (2) is the Brillouin function. In particular, in the limit $I \to \infty$ it takes the form of the Langevin function applicable to dipolar liquids with no H-bonds and for $I = 2$ — the form of hyperbolic tangent applicable to hydrogen bonded liquids at ambient conditions. For small values of the argument Ξ the function can be expanded into the power series:

$$B_I(\Xi) = \frac{I+1}{3(I-1)}\Xi - \frac{I^4-1}{45(I-1)^4}\Xi^3 + \cdots \equiv b(I)\Xi - c(I)\Xi^3 + \cdots. \tag{5}$$

Only the first term in the expansion, the linear term $b(I)\Xi$, is taken into account when one looks for the dielectric constant. The coefficient $b(I)$ and the mean number of orientations I of the dipole moment are interrelated as

$$b(I) = \frac{I+1}{3(I-1)} \tag{6}$$

or inversely

$$I = \frac{3b+1}{3b-1}. \tag{7}$$

According to our proposed statistical model, for small electric fields ($E \sim 10^3$ V m^{-1}), starting from the Brillouin function instead of the Langevin function, one arrives at an expression analogous to the Onsager expression for the dielectric constant ϵ (applicable in its original form to dipolar liquids with no H-bonds), but containing the factor $b(I)$ instead of 1/3:

$$\frac{3\left(\epsilon-n^2\right)\left(2\epsilon+n^2\right)}{\epsilon\left(n^2+2\right)^2} = b(I)\frac{\mu^2 N^0}{\epsilon_0 v k T,} \tag{8}$$

where ϵ_0 is the permittivity of vacuum. The numerical value of $b(I)$ can readily be found from Eq. (8) provided that the other quantities, and in particular the dielectric constant $\epsilon(E \to 0)$, the refraction index n and the number density N^0/v at a given temperature and pressure, are known from experiment. If the experimental data are such that $b(I)$ takes values leading to non-integer values of I (cf. Eq. (7)), the function B_I should be treated as defined by Eq. (2). The physical quantities involved in Eq. (8) needed to find the value of $b(I)$ were found in the literature: T and P values were taken from the vapor–liquid phase boundary data given by Wagner and Pruß [16]. Specific volume v was found from mass density ρ that was also taken from Ref. [16]. To interpolate between the data of the refraction index n_D and, subsequently, between the dielectric constant $\epsilon(E \to 0)$ data found in literature for the chosen (T, P), interpolation polynomials were used [6]. The refraction index n_D (for the wavelength of 0.589 μm) data were taken from Ref. [17]. The values of the dielectric constant $\epsilon(E \to 0)$ come from Ref. [18].

The seventh and eighth columns in Table 1 present the calculated values of $b(I)$ and I, respectively, at temperatures and pressures given

Table 1
Values of the mean number I of allowed orientations of H_2O dipoles and other quantities occurring in Eq. (8) at temperature T and pressure P along the vapor–liquid phase boundary [16].

Nr	$\frac{T}{\mathrm{K}}$ [16]	$\frac{P}{\mathrm{MPa}}$ [16]	$\frac{V}{\mathrm{m^3\ kmol^{-1}}}$ [16]	n_D [17]	$\epsilon\ (E\to 0)$ [18]	$b(I)$ Eq. (8)	I Eq. (7)
1	273.16	0.000612	0.01802	1.33576	87.36	0.9985	2.002
2	300	0.003537	0.01808	1.33200	78.50	0.993	2.0105
3	350	0.041682	0.01850	1.32516	63.46	0.965	2.055
4	400	0.24577	0.01922	1.31264	50.31	0.921	2.134
5	450	0.93220	0.02023	1.29469	39.065	0.865	2.254
6	500	2.6392	0.02167	1.27420	29.72	0.800	2.429
7	550	6.1172	0.02384	1.25048	22.27	0.744	2.623
8	570	8.2132	0.02507	1.23823	19.82	0.731	2.676
9	600	12.345	0.02774	1.21314	16.71	0.738	2.647
10	630	17.969	0.03310	1.17411	14.29[a]	0.831	2.340
11	640	20.265	0.03741	1.15648	12.99[a]	0.932	2.114

[a] Extrapolated.

in the second and third columns, respectively. With these data at hand, the permittivity $\epsilon(T, P, E)$ of water was calculated as follows. Expressing $\langle\cos\theta\rangle$ by the function given by Eq. (2), this time not restricted to the linear approximation in the field, we obtain

$$\epsilon - n^2 = \frac{N^0\mu\left(n^2+2\right)}{3\epsilon_0 vE}\left[\frac{I}{I-1}\coth\frac{I\Xi}{I-1} - \frac{1}{I-1}\coth\frac{\Xi}{I-1}\right]. \quad (9)$$

The quantity Ξ given in Eq. (3), with the notation introduced in Eq. (4) can be written as

$$\Xi = \frac{\mu E}{kT}\frac{\epsilon\left(n^2+2\right)}{2\epsilon+n^2}, \quad (10)$$

or, introducing the Coulomb field

$$E = \frac{q}{4\pi\epsilon\epsilon_0 X^2}, \quad (11)$$

$$\Xi = \frac{q}{4\pi\epsilon_0 X^2}\frac{\mu}{kT}\frac{n^2+2}{2\epsilon+n^2}, \quad (12)$$

where q is the elementary charge, X denotes the reduced radius, $X = r|Z|^{-1/2}$, r is the distance from the center of the ion, and Z is the number of excess elementary charges of an ion.

3. Results

3.1. Permittivity ϵ along the vapor–liquid line

From the vapor–liquid phase boundary [16] eleven points (T, P) were chosen and numbered consecutively in the first column in Table 1. In the current work, we shall refer to the particular points (T, P) by invoking the number of the row in Table 1. Permittivity $\epsilon = \epsilon(T, P, E)$ was calculated on the basis of Eqs. (9) and (10), and $\epsilon = \epsilon(T, P, X)$ was calculated on the basis of Eqs. (9) and (12). The weak electric field $E \sim 10^3$ V m^{-1} applied to measure the dielectric constant is marked as $E \to 0$. At given (T, P), the highest value of ϵ represents the dielectric constant at $E \to 0$. The lowest value of the permittivity ϵ found in the calculations was $\epsilon = 2$ as it should be. The results for $\epsilon = (T, P, E)$ are presented in Figs. 1, 2 and 3, while those for $\epsilon = \epsilon(T, P, X)$ are presented in Figs. 4 and 5. In Figs. 1–5, the lines marked 1 refer to the triple point and bound the bundle of remaining lines from above. The lines marked 11, found for conditions close to the critical point, bound the remaining lines of the bundle from below. Permittivity ϵ decreases monotonously on approaching the critical point from below along the vapor–liquid phase equilibrium line, irrespectively of the field. In Figs. 4 and 5, permittivity $\epsilon = \epsilon(T, P, X)$ increases with increasing reduced radius X. The highest values of $\epsilon = \epsilon(T, P, X)$ are approached asymptotically. Permittivity ϵ decreases monotonously on approaching the critical point while T and P increases, irrespectively of the radius X. In general, the increase in temperature tends to lower the permittivity ϵ [4], whereas an increase in pressure alone has the opposite effect [5]. We find that along the vapor–liquid water phase equilibrium line, permittivity ϵ decreases despite the increase in pressure on approaching the critical point from below.

3.2. Mean number I of allowed orientations of H_2O dipoles

The connection between the number I (Eqs. (7) and (8)) and the H-bonding in water is discussed in Ref. [4]. Originally, the case of $I = 2$ was discussed at ambient conditions referring to two possible orientations of dipole moments during simultaneous shifts in proton positions in H-bonds forming links between neighboring H_2O molecules [4]. This approach is quite general and indeed does apply to any acceptable local structure of liquid water, say, similar to clusters depicted in Ref. [19]. Increasing temperature leads to water with on average less hindered rotation of dipoles of water molecules. In Ref. [4], the mean number I was calculated at isobaric conditions as a function of temperature in the range $273 < T < 373$ K, that is from the freezing point of water to the boiling point at atmospheric pressure. Within this range of temperature, I increases nearly linearly with temperature at a constant pressure (cf. Fig. 6). The isothermal ($T = 293$ K) dependence of the mean number I on pressure increasing up to 900 MPa looks differently (Fig. 7).

The pressure of $P = 900$ MPa is not far from the one at which one encounters the water–ice VI phase transition at ambient temperature. The data for refractive index of water $n(P)$, specific volume of water $v(P)$ and dielectric constant $\epsilon(P)$ were found from the interpolation formulas given in the Appendix to Ref. [5] and used to find the

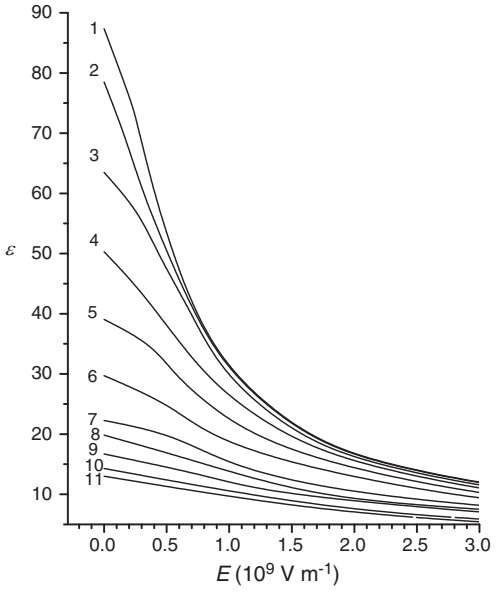

Fig. 1. Permittivity $\epsilon = \epsilon(T, P, E)$ as a function of the electric field strength E for (T, P) points numbered from 1 to 11 (corresponding to the rows in Table 1), chosen at the vapor–liquid phase boundary calculated for E from 0 to 3 GV m^{-1}.

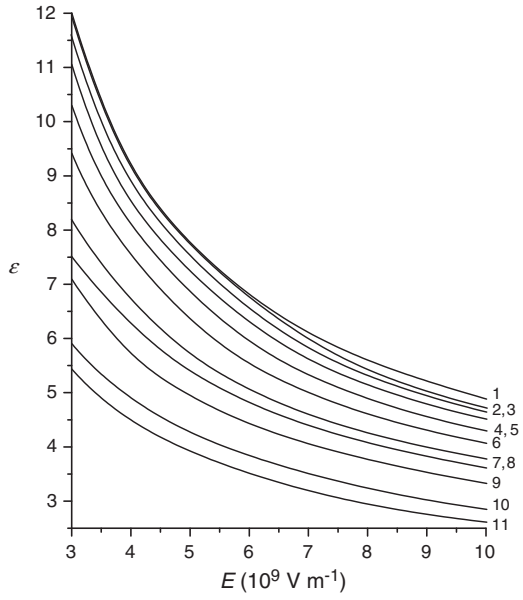

Fig. 2. Same as Fig. 1, but for E from 3 to 10 GV m^{-1}.

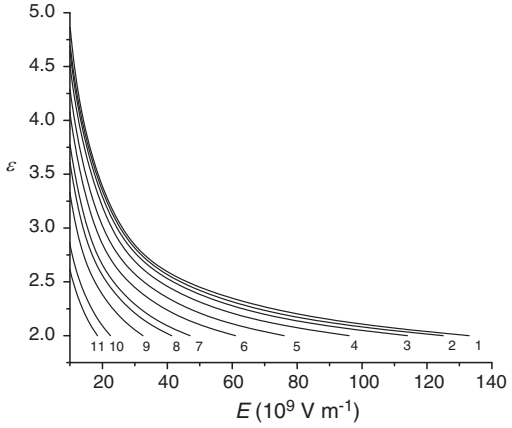

Fig. 3. Same as Fig. 1, but for E from 10 to 140 GV m^{-1}.

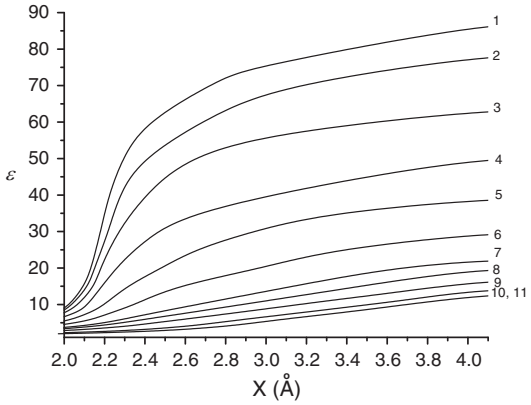

Fig. 5. Same as Fig. 4, but for X from 2.0 to 4.1 Å.

mean number I on the basis of Eqs. (7) and (8) in the pressure range $0.1 < P < 900$ MPa (Fig. 7). In the range 500–900 MPa an extrapolation procedure was applied. It was found that with increasing pressure along the $T = 293$ K isotherm the mean number I increases in the range $0.1 < P < 675$ MPa (Fig. 7), but decreases under higher pressures. It follows that the isothermal dependence $I(P)$ attains a maximum at about $P = 675$ MPa.

In the current work, the behavior of the mean number I is investigated at T and P varied simultaneously, namely for T and P values taken from the vapor–liquid water phase boundary. Starting at the triple point and going along the phase equilibrium line, the mean number I of the allowed orientations of H_2O dipoles increases with increasing temperature and pressure up to the point $T = 570$ K, $P = 8.2$ MPa (cf. Fig. 8), and subsequently decreases. According to our statistical model, higher I values correspond to a higher freedom of rotation of the dipole moments. At the triple point ($T = 273.16$ K, $P = 612$ Pa) and in a proximity ($T = 640$ K, $P = 20.3$ MPa) of the critical point ($T = 647$ K, $P = 22.1$ MPa), I is close to two ($I \cong 2$).

3.3. Dielectric saturation along the vapor–liquid water phase boundary

Dielectric saturation occurs when the dipolar moments $\boldsymbol{\mu}$ of H_2O molecules point along the electric field $\boldsymbol{E}$. Such an effect is characterized by the mean value $\langle\cos\theta\rangle$ very close to the value $\langle\cos\theta\rangle = 1$. Marcus [3] argues that "most of the solvent electrostriction … takes place within … region of dielectric saturation". Sufficiently high electric field around the ions is needed for either effect. Indeed, both descriptions of the state of water in high field as the saturated one and as the one showing huge electrostriction (reduced specific volume) occur at the same conditions, as seen in Ref. [9], Fig. 4 therein. In the high-field E (small radius X) range, $\langle\cos\theta\rangle \cong 1$ and the specific volume d^{-1} (inverse density) of water in the shell decreases with decreasing X, starting with $X \cong 2.19$ Å ($E \cong 1$ GV m^{-1}). In other words, it can be said that "the water molecules in the dielectric saturation region are rotationally immobilized by the field of the ion and their volume is strongly compressed" [3]. Exemplary plots of $\langle\cos\theta\rangle$ vs. E are shown in Fig. 9 for T and P values given in Table 1, rows 1, 8 and 11.

The value of unity is approached asymptotically by $\langle\cos\theta\rangle$ represented by the function defined by Eq. (2) at high E in three different conditions. The mean cosine $\langle\cos\theta\rangle$ is plotted in Fig. 9. For our purposes, we arbitrarily *define* the saturation value E_s at a point where $\langle\cos\theta\rangle + 0.001$ touches the asymptote $\langle\cos\theta\rangle = 1$. E_s denotes the lowest field needed to achieve the dielectric saturation. E_s takes its highest values at $T = 570$ K and $P = 8.2$ MPa. Recall that the mean number I of allowed orientations of H_2O dipoles takes its highest value in the same conditions. It may be interpreted so that most of the deviations of the local structure of water from the tetrahedrally coordinated one is expected at $T = 570$ K and $P = 8.2$ MPa, while close to the triple point and near the critical point the mean number I is close to 2 (Fig. 8) and the local structure is close to the usual tetrahedrally coordinated one.

In Table 2, for three points T, P chosen from the vapor–liquid phase boundary the saturation electric field strength E_s and the corresponding permittivity ϵ_s are given. In the fourth column of Table 2, the radii X_s of the first hydration shells of ions calculated with the use of Eq. (11) are given.

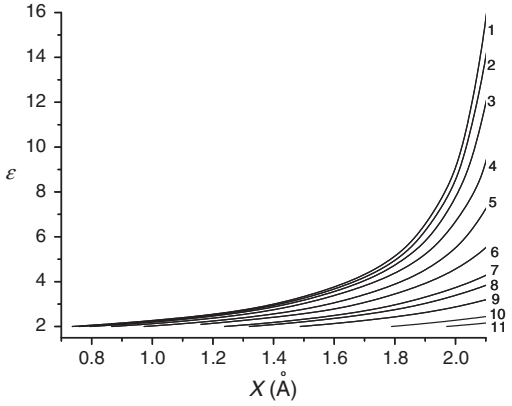

Fig. 4. Permittivity $\epsilon = \epsilon(T, P, X)$ as a function of the reduced distance X from the center of the ion for (T, P) points numbered from 1 to 11 (corresponding to the rows in Table 1), chosen at the vapor–liquid phase boundary calculated for X from 0.7 to 2.1 Å.

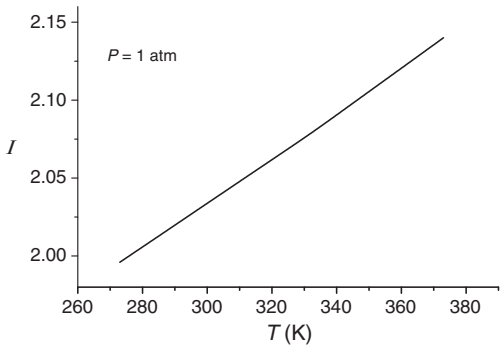

Fig. 6. Mean number I of the allowed orientations of H_2O dipoles as an isobaric function of temperature in the range $273 < T < 373$ K, that is from the freezing point of water to the boiling one, at atmospheric pressure.

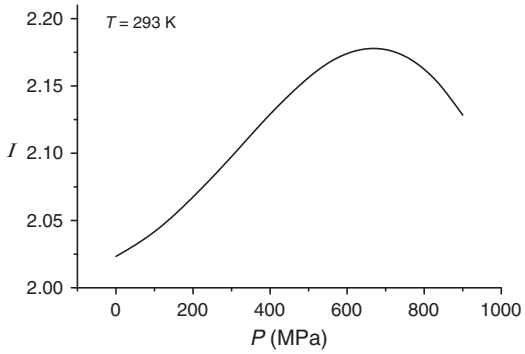

Fig. 7. Mean number I of the allowed orientations of H_2O dipoles as an isothermal function of pressure P in the range $0.1 < P < 900$ MPa at $T = 293$ K.

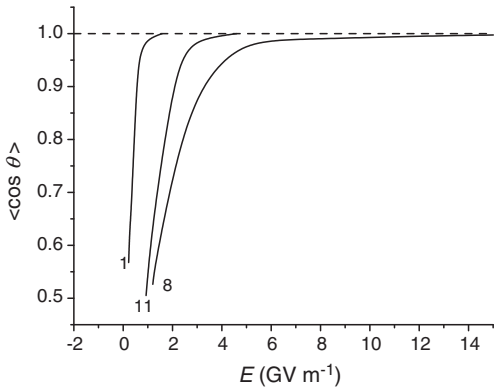

Fig. 9. $\langle\cos\theta\rangle$ as a function of the electric field strength E. Exemplary results of $\langle\cos\theta\rangle$ for temperatures and pressures listed in Table 1, rows 1, 8 and 11.

3.4. Cations with well-defined first hydration shells

In Fig. 10, the values of $\langle\cos\theta\rangle$ are plotted as a function of the reduced radii of the first hydration shells of ions at ambient conditions at $T = 298$ K and $P = 0.1$ MPa (full line a) as well as at $T = 640$ K and $P = 20.3$ MPa (dashed line b), close to the critical state.

Along the full line a, starting with the lowest values of X, that is from ions with very high electric field strengths around them, $\langle\cos\theta\rangle$ shows a nearly constant value very close to unity. For ions with $X < 2.19$ Å, well-defined ion hydration shells are observed in scattering experiments [7,8,20,21]. Note that just at $X = 2.19$ Å a steep decrease in line a begins. The reduced radii of the first hydration shell of Li^+ and the shells of cations doubly, triply and more times charged with the elementary charge fall into the range of $X < 2.19$ Å ($E > 1$ GV m^{-1} at ambient conditions). The exemplary Al^{3+} and Li^+ ions are marked by circles on line a (Fig. 10). Within the first shells of these ions $\langle\cos\theta\rangle \cong 1$. Hence, well-defined ion hydration shells occurring at reduced radii $X < 2.19$ Å are related with the dielectric saturation of hydration water.

3.5. Ions with no well-defined hydration shells at ambient conditions

For the ions HO^-, Na^+, Ag^+, H_3O^+, F^-, K^+, Rb^+, Cs^+, Cl^-, Br^- and I^-, the reduced radii are $X > 2.19$ Å [20–23]. On line a in Fig. 10, $\langle\cos\theta\rangle$ of these ions is marked with triangles. No well-defined ion hydration shells were observed in scattering experiments [7,20,21] at ambient conditions around these ions. It is apparent that for ions with $X > 2.19$ Å the values of $\langle\cos\theta\rangle$ read from the full line a (or Table 3, column 3) lie below unity and hence there is no dielectric saturation in the hydration shells of the latter ions. This is ascribed to relatively weak electric field ($E < 1$ GV m^{-1} at ambient conditions) insufficient to saturate water dipoles in the neighborhood of these ions.

For $2.30 < X < 3.65$ Å (Table 3) at ambient conditions, the mean cosine is confined within the limits $0.91 > \langle\cos\theta\rangle > 0.38$. It means that water in the closest neighborhood of all the ions in Table 3, marked with triangles in Fig. 10, is far from dielectric saturation in such conditions. It may be correlated with the scattering studies of ion hydration [8,21] testifying on the absence of well-defined first hydration shells around the ions of this group. For example, one finds in literature the confirmation of this correlation for K^+. Indeed, from the scattering results it follows that from this list of ions at least the K^+ ion is weakly hydrated [22,24]. Hence, weak hydration of an ion and lack of dielectric saturation in its shell are interrelated. Let us remark that the shells around ions are placed in fields of radial symmetry, hence in the electric saturated state the dipole moments point toward or out of the ion center. According to Refs. [22,24], the orientation of the dipole moments of water molecules in the hydration shell of K^+ is not radial or, which is equivalent, not along the K^+-water oxygen director. In particular, Fig. 6 in Ref. [24] shows a rather wide distribution of the angles θ between the potassium ion–water oxygen director and the water molecule dipole moment. This is just what we call lack of saturation.

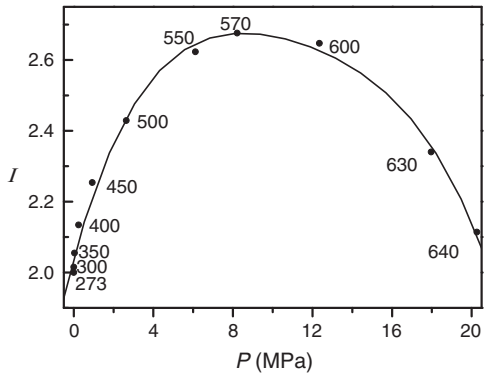

Fig. 8. Mean number I of the allowed orientations of H_2O dipoles as a function of pressure P along the vapor–liquid phase boundary. The numbers at the points denote absolute temperatures (in K).

3.6. HO^-, Na^+, Ag^+, H_3O^+, F^-, K^+, Rb^+, Cs^+, Cl^-, Br^- and I^- ions close to critical conditions

At $T = 640$ K and $P = 20.3$ MPa, that is in conditions at the vapor–liquid water equilibrium and not far from the critical point, for some ions the situation is different (Fig. 10, line b and Table 3). In this case, even for the radii $2.30 < X < 2.63$ Å dielectric saturation $\langle\cos\theta\rangle \cong 1$ is possible. Hence, the nearly-critical conditions are favorable for the formation of well-defined, saturated hydration shells around the ions with $X = X_s$, in particular HO^-, Na^+, Ag^+, H_3O^+ and F^-. However, the state of water in the neighborhood of the K^+, Rb^+, Cs^+, Cl^-, Br^- and I^- ions is not electrically saturated even in conditions close to the critical point (Table 3).

By varying T and P in certain ways, one can pass from the case of no well-defined hydration shells at ambient conditions to the one with well-defined shells of the same ions [2]. This is due to the fact

Table 2
Electric field strength E_s at saturation, permittivity ϵ_s and reduced hydration shell radii X_s characterizing the limits of dielectric saturation $\langle\cos\theta\rangle \cong 1$. The numbers marking the rows correspond to the conditions T and P in Table 1.

Nr	$\frac{E_s}{\text{GV m}^{-1}}$	ϵ_s	$\frac{X_s}{\text{Å}}$
1	1.5	23	2.04
8	15	2.7	1.88
11	4.5	4.2	2.76

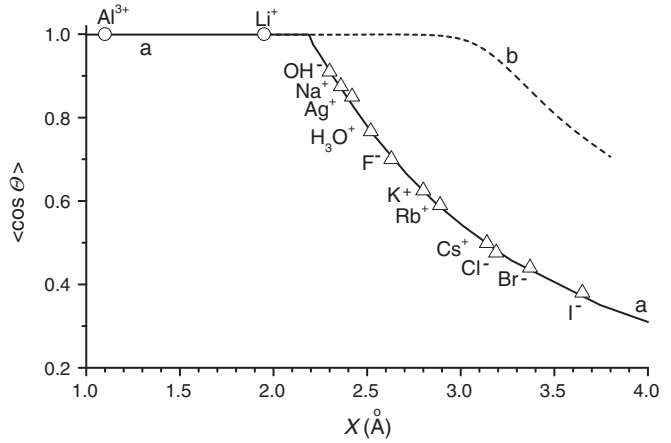

Fig. 10. ⟨cosθ⟩ as a function of the reduced radius X of the first hydration shell of an ion; a — full line at ambient conditions ($T = 298$ K, $P = 0.1$ MPa), b — broken line at $T = 640$ K and $P = 20.3$ MPa close to the critical point. Exemplary ions with known well-defined hydration shells: Al^{3+} and Li^+ are marked by circles (○) on line a. Data for monovalent cations and anions with no well-defined hydration shells found experimentally are marked by triangles (Δ) on line a.

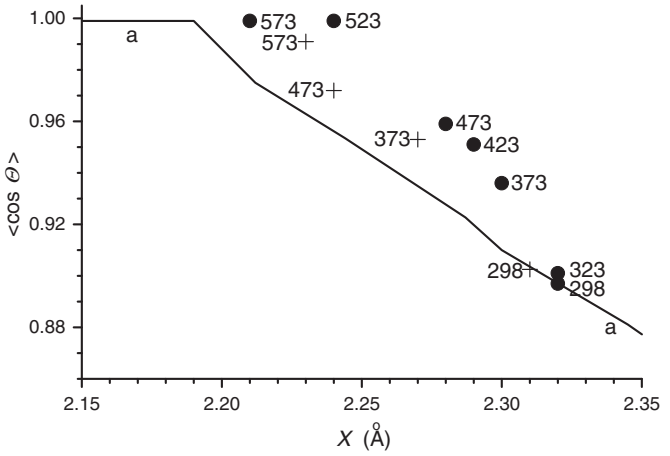

Fig. 11. ⟨cosθ⟩ as a function of the reduced radius X of the first hydration shell of ions; a — full line at ambient conditions ($T = 298$ K, $P = 0.1$ MPa). Full circles (●) denote ⟨cosθ⟩ of estimated data for Ag^+ ions in 0.01 m $AgNO_3$ aqueous solution along the vapor saturation line (radii X from Table 1 in Ref. [10]) measured at several temperatures. Numbers to the right of the circles denote the temperatures in K, for which in Ref. [10] the radii X were found. Note that dielectric saturation ⟨cosθ⟩ ≅ 1 is reached at temperatures 523 K and 573 K. Crosses (+) denote the same function for Ag^+ ions in 0.10 m $AgClO_4$ aqueous solution (radii from Table 2 in Ref. [10]) measured at several temperatures. Numbers to the left of the crosses denote the temperatures in K, for which in Ref. [10] the radii X were found. Note that in the latter case dielectric saturation is approached, but not attained.

that with varying T and P the electric field E acting on the shells varies, too. Firstly, E depends on the reduced radius $X(T, P)$ of the shell, which can be inferred from experiment. Secondly, E depends on the permittivity of water $\epsilon(T, P)$, which we are able to calculate. However, since data on hydration shells of ions at elevated temperatures and pressures are scarce, only a limited comparison of the current calculations concerning that group of ions with the experimental data is possible. What we found in the literature concerned Ag^+ and Rb^+.

Seward et al. [10] investigated hydrated Ag^+ ions at various temperatures between 298 and 573 K at equilibrium saturated vapor pressures, that is along the liquid water–saturated vapor line, by extended X-ray absorption fine structure (EXAFS) measurements. Values of ⟨cosθ⟩ estimated in the current work for Ag^+ ions in 0.01 m $AgNO_3$ and 0.10 m $AgClO_4$ aqueous solutions were based on the hydration shells radii X given in Ref. [10], Tables 1 and 2 therein, respectively. In Fig. 11, full circles denote ⟨cosθ⟩ for the former data. Note that dielectric saturation ⟨cosθ⟩ = 1 is reached. Crosses (+) denote ⟨cosθ⟩ for the latter data. Note that in the latter case dielectric saturation is approached, but not reached.

They [10] found that with increasing temperature the Ag – O bond length decreased by about 0.10 Å. It follows from our considerations that not far from 573 K the hydration shells of Ag^+ are in the electric saturated state (cf. Fig. 11, full circles) and one should expect that the contracted shells are well-defined. Actually, it might be suspected that data defining the character of the first shells were already available in the experiment [10], but only the question if the shells were well-defined or not was not expressed verbally. Anyway, even if this is the case, the latter expectation must still wait for an immediate experimental confirmation (but compare the case of Rb^+ discussed thereafter).

Fulton et al. [2] performed X-ray absorption fine structure (XAFS) measurements for Rb^+ in supercritical ($T = 697$ K and $P = 38.2$–63.3 MPa) water solutions. They found a slight reduction in the Rb – O distance by about 0.10 Å when going from ambient to supercritical conditions. Other XAFS results [25] also indicate gradual reduction in the Rb – O distance with temperature increasing from ambient to 448 K under a pressure of 3 MPa. Fulton et al.'s [2] XAFS results indicate that well-defined hydration shells (or, in other words, contracted shells of tightly-bound, well-ordered water [2]) are formed around Rb^+ cations even at 697 K. The reduction in the ion–O distance could be opposed by steric hindrances, but in the conditions of elevated temperature this can be avoided, since the coordination numbers of the ions are reduced, at least for Ag^+ [10] and Rb^+ [2,25].

We have to do with rather simple physics. If for any reason the distance from the center of an ion to a H_2O molecule is shortened, it becomes subdued by the action of a higher Coulomb field, which favors the dielectric saturation. It concerns not only the ion center–oxygen distances when going from one ion to another of different dimensions, as exemplified in Fig. 10, but also a specific ion whose ion–O distance was reduced due to increasing temperature and pressure. In other words, water approaches the saturation state either when going from an ion with longer X to an ion with shorter X, or by reducing (contracting) the ion shell radius by increasing T and P. Although our calculations and plots concern at most subcritical conditions, it seems likely to us that this simple reasoning can be extended to the supercritical conditions as well. The results presented in Ref. [2] reveal the shortening of the Rb^+ – O bond in supercritical conditions with respect to that at the ambient ones. This is accompanied with a formation of well-defined hydration shells in supercritical conditions. This is not the case at ambient conditions. Note that according to that simple reasoning this is qualitatively consistent with our results despite the fact that our calculations do not reach the highest temperatures and pressures applied in Ref. [2].

Table 3
Reduced hydration shell radii X of ions at ambient conditions ($T = 298$ K, $P = 0.1$ MPa) and ⟨cosθ⟩ of the first shell of water around them at ambient conditions and in conditions $T = 640$ K and $P = 20.3$ MPa close to the critical state. X is approximately taken as independent on T and P. The list of ions that are surrounded by electrically saturated shells at nearly critical conditions and thus are likely to form well-defined shells at such conditions begins at the top of the table and ends with the row with the underlined number in the last column.

Ion	$\frac{X_s}{\text{Å}}$	⟨cosθ⟩ ambient	⟨cosθ⟩ nearly critical
HO^-	2.30 [22]	0.910	0.999
Na^+	2.36 [20]	0.875	0.999
Ag^+	2.42 [20]	0.850	0.999
H_3O^+	2.52 [21]	0.767	0.999
F^-	2.63 [20]	0.700	0.999
K^+	2.80 [20]	0.625	0.998
Rb^+	2.89 [20]	0.590	0.997
Cs^+	3.14 [20]	0.499	0.971
Cl^-	3.19 [20]	0.476	0.940
Br^-	3.37 [20]	0.440	0.870
I^-	3.65 [20]	0.380	0.750

4. Discussion and summary

In the current work, three essential goals were achieved. Firstly, new data for static electric permittivity $\epsilon(T, P, E)$, not immediately accessible from experiment, were calculated. Further on, a quantitative measure of the phenomenon of dielectric saturation was introduced and applied to the hydration shells of a number of ions. At last, two categories of ions were discerned: one with first hydration shells electrically saturated and another with no saturation in them. This was correlated with the presence of well-formed first hydration shells of ions, as observed in scattering experiments, or a lack of such shells, respectively.

The experimental values of permittivity ϵ in the fields of strength $E > 10^7$ V m^{-1} encountered in the shells are currently not immediately available from experiment, so only the theory can provide them. Under atmospheric pressure and in the temperature range $273 < T < 373$ K such ϵ data are given in Ref. [4]. At ambient temperature and under pressures in the range $0.1 < P < 600$ MPa such ϵ data are provided in Ref. [5]. In the current paper, data for $\epsilon = \epsilon(T, P, E)$ are calculated at T and P varied simultaneously, namely for temperature and pressure values taken from the vapor–liquid water phase boundary. In addition, we calculated $\epsilon = \epsilon(T, P, E)$ at ambient T and P varied up to 900 MPa; these data are not explicitly given herein, but used to calculate the quantity I (Fig. 7). Hence, the current work provides new theoretical results — the calculated values of permittivity ϵ in conditions not exploited yet.

In high fields, the phenomenon of dielectric saturation in water is encountered. Qualitatively, according to literature, "the water molecules in the dielectric saturation region are rotationally immobilized by the field of the ion" [3]. In the current work, we introduce a quantitative measure of the saturation phenomenon. Namely, by definition, we admit that a state of dielectric saturation is reached from below if the value of $\langle\cos\theta\rangle = 1$–0.001 is attained.

The physical conditions needed to achieve dielectric saturation in water are nearly the same as those giving rise to a huge electrostriction. At ambient conditions, it is well illustrated in Fig. 4 in Ref. [9], where the electric field range (or, equivalently, the radius of the hydration shell of an ion) at which $\langle\cos\theta\rangle \cong 1$ is almost the same as that for which, due to the huge electrostriction, the reciprocal relative water density d^{-1} is markedly reduced below its usual value of unity. For example, for the water shells around Li^+ ions one finds $d^{-1} = 0.83$, and $d^{-1} = 0.37$ in the case of Al^{3+} ions at ambient conditions [9]. A part of our current data of $\epsilon = \epsilon(T, P, E)$ from 398 K up to 473 K along the water–vapor saturation line, made available by us to the author of Ref. [3] prior to our writing of the current paper, were used by him, with due reference, to find the electrostricted water regions around ions characterized by electric saturation in the qualitative sense quoted above. Our full current data of $\epsilon = \epsilon(T, P, E)$ for $273 < T < 640$ K and 0.61 kPa $< P <$ 20.3 MPa, i.e., from the triple point to nearly critical conditions along the water–vapor equilibrium line, are used herein to find, among other things, $\langle\cos\theta\rangle$ and the conditions for quantitatively conceived saturation $\langle\cos\theta\rangle \cong 1$ for ion hydration shells.

In aqueous solutions, ions with the reduced radii $X < 2.19$ Å of their first hydration shells, for example those with the shell radii X comprised between those of Al^{3+} and Li^+ [9], have well-defined hydration shells around them at ambient conditions. Their well-defined hydration shells were found by X-ray and neutron scattering methods [8,20,21]. On the other hand, according to our calculations, water in their shells is at ambient conditions electrically saturated, i.e., $\langle\cos\theta\rangle \geq 1$–0.001 in the fields $E > 1$ GV m^{-1}. It is illustrated in Fig. 10, see the nearly horizontal part of full line a. Ions with the radii of their shells between those of Al^{3+} and Li^+ are not explicitly shown. On the contrary, the shells around ions with $X > 2.19$ Å that according to scattering studies are not well-defined, are also not electrically saturated. This is exemplified by the shells of ions of radii comprised between those of Na^+ and I^- (cf. Fig. 10, see the ions marked by triangles on the descending part of full line a). In particular, the shells about K^+ ions, with $X = 2.63$ Å at ambient conditions are not well-defined (see Refs. [7,24]).

If temperature and pressure of aqueous solutions increase up to the values $T = 640$ K and $P = 20.3$ MPa not far from the critical ones, then even the ions with $2.19 < X < 2.63$ Å can have well-defined hydration shells. According to our calculations, their first shells at higher T and P become electrically saturated (cf. Fig. 10 dashed line b and Table 3). Indeed, for Ag^+ [10] and Rb^+ ions [2,25], it was found that with increasing T and P above the ambient conditions slight contractions of the first shell radii are observed together with a tendency to form well-defined hydration shells, the latter at least around Rb^+. In Fig. 11, it is shown how water in the first shells of Ag^+ ions in $AgNO_3$ solutions, with the radii X measured with increasing T and P along the vapor–liquid water line [10], attains dielectric saturation $\langle\cos\theta\rangle \cong 1$. Note that in the analogous case, for shells of Ag^+ in $AgClO_4$ solutions, dielectric saturation is approached, but not reached. We expect that like the shells of many ions at ambient conditions and Rb^+ ions [2] at higher T and P, Ag^+ ions should also form well-defined shells in conditions in which water becomes electrically saturated.

5. Conclusion

In the current work, the problem of dielectric saturation of water in high electric fields exceeding 1 GV m^{-1} at elevated temperature and pressure was investigated in the context of simple ion hydration. In particular, conditions necessary for observing well-defined hydration shells were discussed in this context. The essence of our argument lies in discussing the dielectric properties of the hydration shells that provide a criterion in predicting the presence or absence of the well-defined structure of their radial distribution function as observed with the help of X-rays or neutrons. It is concluded that well-defined hydration shells can be observed at the same conditions along with their state of dielectric saturation. This conclusion is based on a comparison of our calculations concerning dielectric saturation in the shells with literature data on the radial distribution functions of water around ions. A prediction is formulated that ions with no well-defined hydration shells at ambient conditions may get such shells at high temperature and pressure if dielectric saturation of water around them is attained.

Acknowledgment

The authors express their thanks to Professor Yizhak Marcus for bringing the problem of high-field static electric permittivity at water–vapor equilibrium conditions to their attention.

References

[1] C. Da Silva-Cadoux, J.-L. Hazemann, D. Testemale, O. Proux, C. Rochas, Journal of Chemical Physics 136 (2012) 044515.
[2] J.L. Fulton, D.M. Pfund, S.L. Wallen, M. Newville, E.A. Stern, Ma Yanjun, Journal of Chemical Physics 105 (1996) 2161.
[3] Y. Marcus, The Journal of Physical Chemistry. B 116 (2012) 7232.
[4] I. Danielewicz-Ferchmin, A.R. Ferchmin, Physical Chemistry Chemical Physics 6 (2004) 1332.
[5] E. Banachowicz, I. Danielewicz-Ferchmin, Physics and Chemistry of Liquids 44 (2006) 95.
[6] I. Danielewicz-Ferchmin, A.R. Ferchmin, Acta Physicae Superficierum (Łódź–Poznań) 12 (2012) 44.
[7] I. Howell, G.W. Neilson, P. Chieux, Journal of Molecular Structure 250 (1991) 281.
[8] J.E. Enderby, Chemical Society Reviews 24 (1995) 159.
[9] I. Danielewicz-Ferchmin, A.R. Ferchmin, Physica B: Condensed Matter 245 (1998) 34, (and references cited therein).
[10] T.M. Seward, C.M.B. Henderson, J.M. Charnock, B.R. Dobson, Geochimica et Cosmochimica Acta 60 (1996) 2273.
[11] I. Danielewicz-Ferchmin, A.R. Ferchmin, Journal of Molecular Liquids 124 (2006) 114.
[12] K.A. Maerzke, J.I. Siepmann, Journal of Physical Chemistry 114 (2010) 4261.
[13] J.L. Aragones, L.G. MacDowell, J.I. Siepmann, C. Vega, Physical Review Letters 107 (2011) 155702.
[14] Y. Marcus, Journal of Molecular Liquids 79 (1999) 151.
[15] C.J.F. Böttcher, O.C. Van Belle, P. Bordevijk, A. Rip, Second revised edition, Theory of Electric Polarization, vol. 1, Elsevier, Amsterdam, 1973.

[16] W. Wagner, A. Pruß, Journal of Physical and Chemical Reference Data 31 (2002) 387.
[17] A.H. Harvey, J.S. Gallagher, J.M.H. Levelt Sengers, Journal of Physical and Chemical Reference Data 27 (1998) 761.
[18] D.P. Fernandez, A.R.H. Goodwin, E.W. Lemmon, J.M.H. Levelt Sengers, R.C. Williams, Journal of Physical and Chemical Reference Data 26 (1997) 1125.
[19] D. Rai, A.D. Kulkarni, S.P. Gejji, L.J. Bartolotti, R.K. Pathak, Journal of Chemical Physics 138 (2013) 044304.
[20] Y. Marcus, Chemical Reviews 88 (1988) 1475.
[21] M. Magini, G. Licheri, G. Paschina, G. Piccaluga, G. Pinna, X-ray Diffraction of Ions in Aqueous Solutions, CRC Press, Inc., Boca Raton, Florida, 1988.
[22] S. Imberti, A. Botti, F. Bruni, G. Cappa, M.A. Ricci, A.K. Soper, Journal of Chemical Physics 122 (2005) 194509.
[23] Y. Marcus, Journal of Chemical Physics 137 (2012) 154501.
[24] A.K. Soper, K. Weckström, Biophysical Chemistry 124 (2006) 180.
[25] M. Shibukawa, M. Harada, T. Okada, Y. Ogiyama, T. Shimasaki, Y. Kondo, A. Inoue, S. Saito, RSC Advances 2 (2012) 8985.